Nuclear Materials and Energy 8 (2016) 1–7

Contents lists available at ScienceDirect

Nuclear Materials and Energy

journal homepage: www.elsevier.com/locate/nme

Sputtering of iron, chromium and tungsten by energetic deuterium ion bombardment

K. Sugiyama, K. Schmid, W. Jacob*

Max-Planck-Institut für Plasmaphysik, Garching, D-85748 Germany

ARTICLE INFO

Article history:
Available online 25 June 2016

PACS:
52.40Hf
28.52.Fa
68.49Sf
79.20.Rf

Keywords:
Ion sputtering
RAFM steel
Plasma-material interactions

ABSTRACT

Sputtering of the pure materials iron (Fe), chromium (Cr) and tungsten (W) due to energetic deuterium (D) ion bombardment was investigated. These materials are important constituents of reduced-activation ferritic-martensitic steels. Sputtering yields were measured as a function of the D ion energy from 60 to 2000 eV/D. The obtained data can be well reproduced by a semi-empirical formula suggested by Bohdansky, and the corresponding fitting parameters are provided. It is confirmed that analytical formulae suggested by Eckstein and Yamamura agree satisfactorily with these experimental data. By comparison with results from the binary-collision-approximation-based calculation codes SDTrimSP and SRIM it is found that SRIM has some limitations in simulating sputter yield close to the threshold whereas SDTrimSP results show good agreement with measured data in the investigated energy range.

1. Introduction

Sputtering of plasma-facing materials due to interaction with energetic ions (particularly hydrogen isotopes) is an essential issue in magnetically confined fusion devices because it is directly related to impurity generation as well as to the lifetime of plasma-facing components [1]. Sputtering behavior of candidate materials, such as beryllium and carbon, due to energetic hydrogen isotope ion bombardment was extensively studied in the last several decades [2]. Reduced-activation ferritic-martensitic (RAFM) steels, such as EUROFER [3], RUSFER [4], the Japanese alternative F82H [5] or the Chinese CLAM [6] which are being developed as structural materials for fusion applications, are recently also considered as a possible option for certain areas of plasma-facing surfaces in a future power plant because of technological and economic advantages [7]. This has triggered the evaluation of EUROFER steel erosion by energetic deuterium (D) bombardment [8]. Sputtering of RAFM steel is more complex than for pure elements because steel is a compound material. For example, one can theoretically expect that lighter alloyed elements will be preferentially sputtered, leading to a continuous change of the surface stoichiometry during ion irradiation until a steady state is reached. For a better understanding of the sputtering processes on RAFM steels it is in a first step necessary to know the sputtering of each alloyed element as a reference. However, sputtering data for these elements are still quite limited. A few data for iron and tungsten exist, but for chromium no experimental data are available.

In this study we, therefore, measure the sputtering yields of some of the key elements for RAFM steels, i.e. iron (Fe: the base material), chromium (Cr: the second major alloyed element (~ 10 at.%)) and tungsten (W: the highest-Z admixed element in RAFM steels), under well-defined conditions in order to obtain comprehensive data sets for these constituents. Particular emphasis was put on measuring data close to the threshold for physical sputtering. Thin sputter-deposited films were used in this study because they offer the principal advantage to measure sputter yields with higher sensitivity. For thin films the change in layer thickness after sputtering can be measured with ion beam analysis methods. This procedure allows measuring yields with higher sensitivity than, e.g., weight loss measurements. In this work, results from weight loss measurements are compared with those from ion beam analysis. The obtained data are evaluated with fitting formulae for a parametrization and analytic description of the measured sputtering yields. Furthermore, the experimental data are compared with existing sputtering simulation codes for benchmarking. This step is essential because the erosion rate of steel walls in future fusion devices will be eventually assessed numerically by using such simulation codes.

* Corresponding author.
E-mail address: wolfgang.jacob@ipp.mpg.de (W. Jacob).

http://dx.doi.org/10.1016/j.nme.2016.05.016

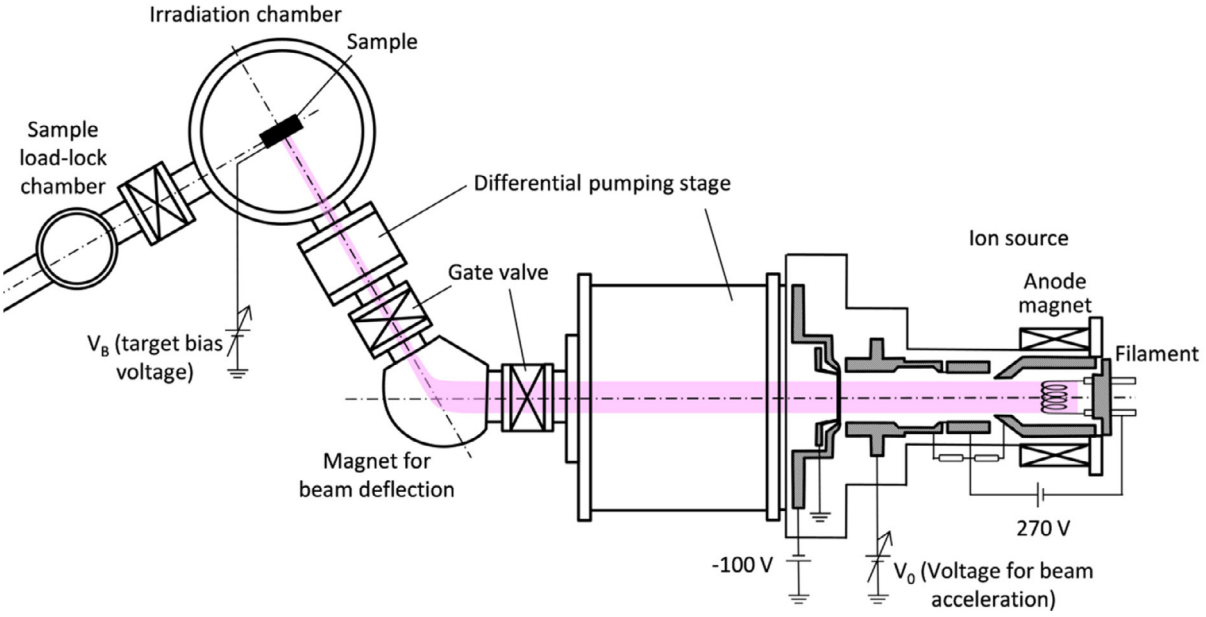

Fig. 1. Schematic view of the high-current ion source set-up [9].

2. Experimental procedure

2.1. Sample preparation

Thin layers of Fe, Cr and W were prepared by magnetron-sputter deposition using a UNIVEX 450B device (Leybold Vacuum GmbH). Single-crystalline silicon (Si) wafers were used as substrates. The sample dimensions were 12 mm × 15 mm. In order to ensure the layer adhesion the Si substrate surface was cleaned by argon (Ar) RF plasma etching for 1 min. prior to the layer deposition. Ar was also used as working gas during deposition at a pressure of 0.3 Pa. The background pressure inside the deposition chamber is $\sim 2–3\times10^{-5}$ Pa. A high power DC-discharge was applied for the magnetron-sputtering of the target (600 W for Fe and Cr, and 300 W for W deposition). The deposition rate was roughly 20 nm/min and the thickness of the deposited layers was 350–400 nm. No bias voltage was applied to the substrate holder. Under these deposition conditions the Ar content in the deposited layers is below the detection limit of the applied ion-beam analysis (see below). In each deposition run a graphite substrate was coated together with the Si substrates. This allows the measurement of low-Z impurities, such as oxygen (O), in the layers by Rutherford backscattering. The determined O concentrations in the layers were about 2–3 at.% for Fe and W and about 5–6 at.% for Cr.

2.2. Deuterium ion irradiation

Prepared specimens were then irradiated by D ions in the high-current ion source set-up (HSQ) at IPP Garching [9]. The HSQ set-up consists of a duo-PIGatron type ion source [10], two differential pumping stages, a sector magnet for beam deflection and a target irradiation chamber connected to a load-lock chamber, as schematically shown in Fig. 1. The sector magnet enables to provide a mass-separated D ion beam at defined ion energy, which is well suited for well-defined sputtering yield measurements. The D energy can be controlled by the ion acceleration voltage and the sample biasing. The dominant ion component generated in the ion source is D_3^+. This ion was chosen as the bombarding species to achieve higher particle fluxes. These molecular D_3^+ ions are considered to be identical to 3 individual D ions impinging with the same velocity as the molecular ion. Correspondingly, the energy per deuteron is 1/3 of the experimentally applied ion energy and the flux is three times the measured ion flux. In this study, the sputtering yield was measured in the D energy range from 60 to 2000 eV/D. The ion beam incident angle was normal to the sample surface.

The ion bombardment induces some change of the surface morphology resulting in the appearance of a visible “footprint” of the D ion beam. The ion beam spot area was determined by measuring the footprint size. It varies from 0.3 to 0.85 cm^2 depending on the D energy. The experimental ion fluxes and fluences were calculated from the measured ion currents and beam spot areas. This includes the implicit assumption that the beam intensity is relatively homogeneous across the beam spot. In fact the variation of irradiation beam intensity was checked by measuring the lateral erosion profile after the D irradiation by scanning the ion-beam analysis beam spot over the sample. The ion-beam analysis beam spot size is about 1 mm^2 and, therefore, significantly smaller than the D irradiation beam spot. The such-determined variation of the current density over the beam spot is of the order of 10 to 20 %. The determined area size is expected to include 10 – 20 % of measurement error. This uncertainty of the beam flux and profile affects the determination of the local beam flux and fluences and the evaluation of the RBS data (see below) but not the evaluation of the weight loss measurements. The ion beam current at the target is typically $\sim 10^{-5}$ A, corresponding to a deuteron flux of $\sim 10^{19}$ $Dm^{-2}s^{-1}$. The irradiation fluences in this work were varied in the range of $1–3\times10^{23}$ Dm^{-2} corresponding to exposure durations between 3 and 9 h. Since the background pressure in the target irradiation chamber is sufficiently low ($\sim 10^{-6}$ Pa), surface oxidation during irradiation is not expected. The sample was not actively cooled during irradiation, resulting in slight temperature rise to 310 up to 360 K depending on the ion impinging energy.

2.3. Post-irradiation analyses

The sputtering yield was evaluated by weight-loss (WL) technique and Rutherford Backscattering Spectrometry (RBS). For WL, the sample weight was measured ex-situ before and after D irradiation by a microbalance system (Sartorius MC21S) having a weight resolution of 1 μg and the measurement uncertainty of ± 3 μg. The sputtering yield was then calculated from the weight loss and the

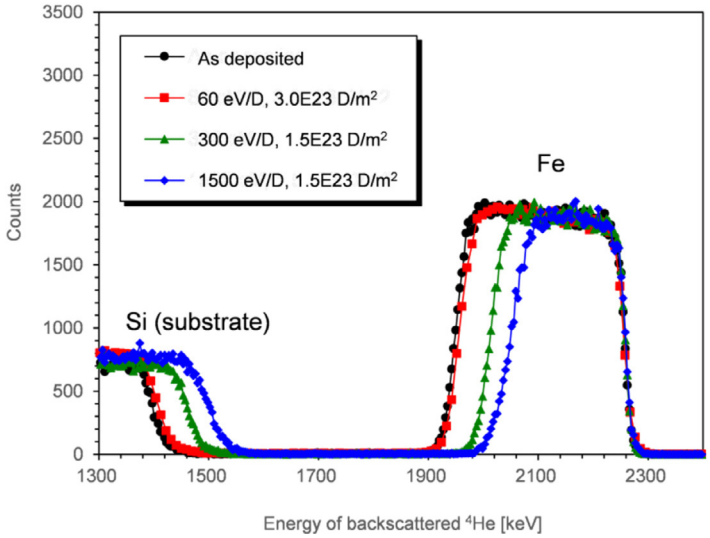

Fig. 2. RBS spectra obtained from Fe layer (on Si substrate) samples before (as deposited) and after D ion irradiation with different irradiation conditions. The primary energy of the ^{4}He beam was 3.0 MeV. The backscattered ^{4}He was measured by a detector located at the laboratory angle of 165°.

total number of impinged D atoms. The measurement error for WL was estimated from the above mentioned measurement uncertainty and the uncertainty of the beam current measurement. For D irradiation energies near the threshold energy for sputter erosion, higher D fluences were accumulated to achieve sufficient weight changes. Nevertheless, the weight loss was in these cases relatively small (around 10 µg), resulting in a larger relative error. On the other hand, the relative error becomes smaller in the higher energy range where sufficient weight losses were usually obtained (up to ~ 50 µg).

RBS measurements were performed using 3.0 MeV ^{4}He ions as probe beam. The ^{4}He$^+$ beam was provided by a 3 MV Tandem accelerator connected to an ion beam analysis chamber. A beam aperture in front of the sample limits the ^{4}He$^+$ irradiation spot size to 1 mm × 1 mm at the sample surface, meaning that the ^{4}He$^+$ beam size is sufficiently smaller than the D beam footprint. The RBS measurements were performed in the center of the D ion irradiation spot. The backscattered ^{4}He$^+$ was analyzed by a solid state detector located at an angle of 165°. Fig. 2 shows examples of RBS spectra obtained from a Fe layer before and after D ion irradiation using various irradiation conditions. Backscattering from the thin Fe layer gives rise to the rectangular-shaped peak in the backscatter-energy range of about 1950 to 2300 keV. The highest backscatter energy (about 2300 keV) is from backscattering at the Fe surface and the thickness of the Fe layer is characterized by the width of this peak. Backscattering from the silicon substrate produces the step visible at lower energy. Because projectile ions reaching the interface have to travel through the Fe layer at the sample surface they experience an energy loss depending on the thickness of the Fe layer. As a result, the position of the Si step depends on the thickness of the Fe layer and changes in close correspondence to the width of the Fe peak. As can be seen in Fig. 2 the layer thickness of the Fe layer changes by D irradiation depending on the D ion energy and fluence. Each RBS spectrum was evaluated with the SIMNRA program [11] to quantitatively determine the thickness change. The sputtering yield was then determined from the thickness change and the D ion fluence. The RBS setup used in this study is well calibrated and the experimental uncertainty is expected to be ~ 10 %. In practice it is difficult to determine thickness changes of less than 10^{16} at./cm^2. Therefore, this value is taken as the minimum absolute uncertainty for RBS. Consequently, for cases where the thickness change is small the absolute uncertainty becomes comparable with this detection limit and the relative uncertainty becomes large. As mentioned above, the D fluence was determined by measuring the total accumulated D ion charge and the beam footprint area assuming a homogeneous ion flux across the footprint. The uncertainty of the determination of the footprint area (see above) was taken into account in the calculation of sputter yields from the RBS data. The total uncertainty associated with the RBS data evaluation was finally estimated using common error propagation taking those technical uncertainties of the RBS and the ion fluence calculation into account.

3. Results and discussion

3.1. Experimental results and the yield curve fitting

Fig. 3 shows sputtering yield data of each element as a function of the D bombardment energy. Additionally, the data are summarized in Table 1. By and large, the sputtering yields measured by weight loss (WL) and by RBS agree within the experimental uncertainties. However, at the higher ion energies (> 5 times the threshold energy), where the error bars are smaller, a systematic small deviation between both methods becomes apparent. The RBS-measured yields are slightly higher than the WL yields. This can be explained by the additional uncertainties in the RBS evaluation due to the possible peaking of the beam profile and the determination of the precise beam area as discussed in Sect. 2.3. Because the RBS data are measured in the center of the irradiation beam spot a peaking would lead to a higher local fluence than the calculated mean fluence. In the evaluation, this would lead to slightly higher yield. For the evaluation of the WL data this effect does not occur. For this reason, we consider the weight-loss data at the higher energies more reliable. On the other hand, the RBS measurements are advantageous at low energies where the yields are low. In this region the evaluation of the WL data suffers from a much larger uncertainty.

Available literature data for Fe and W [9] are also shown in the figure. The present data are comparable with the published data within the experimental uncertainty, but they are systematically higher (for W up to a factor of 2). The reason for that is not clear. One difference is that the previous studies were performed using polycrystalline bulk samples, whereas sputter-deposited thin layers were used in this study. Although we do not anticipate that

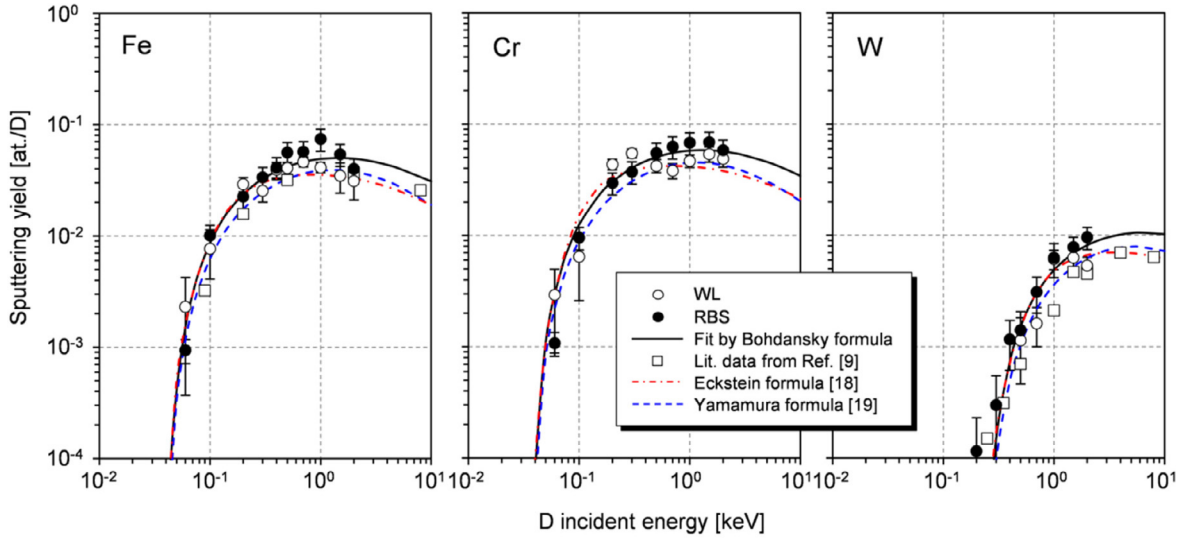

Fig. 3. Experimentally determined sputtering yields of Fe, Cr and W. The solid curve is derived from the fitting by Bohdansky formula [12]. For Fe and W, literature data [9] are also shown. The dashed yield curves are from the analytical formulae by Eckstein [18] and Yamamura [19]. For the formulas, see also the Appendix.

Table 1
Sputtering yield data of Fe, Cr and W experimentally determined in this study. "WL" stands for the data determined by weight-loss measurement whereas "RBS" is by Rutherford Backscattering spectrometry. The value in round brackets shown next to each yield value is the estimated absolute error.

D energy [keV]	Fe				Cr				W			
	WL (error)		RBS (error)		WL (error)		RBS (error)		WL (error)		RBS (error)	
0.06	2.30E−3	(1.9E−3)	9.4E−4	(2.3E−4)	2.92E−3	(2.0E−3)	1.08E−3	(2.6E−4)				
0.1	7.69E−3	(3.6E−3)	0.0101	(2.3E−3)	6.46E−3	(3.9E−3)	9.56E−3	(2.2E−3)				
0.2	0.0292	(4.3E−3)	0.0226	(5.1E−3)	0.0435	(4.8E−3)	0.0297	(6.7E−3)				
0.3	0.0255	(5.4E−3)	0.0336	(7.5E−3)	0.0546	(5.1E−3)	0.0373	(8.4E−3)			3.0E−4	(2.5E−4)
0.4	0.0394	(6.4E−3)	0.0412	(9.2E−3)							1.17E−3	(5.5E−4)
0.5	0.0407	(5.0E−3)	0.0563	(1.3E−2)	0.0422	(5.7E−3)	0.0549	(1.2E−2)	1.14E−3	(6.8E−4)	1.41E−3	(6.4E−4)
0.7	0.0463	(4.7E−3)	0.0571	(1.3E−2)	0.0381	(5.9E−3)	0.0626	(1.4E−2)	1.62E−3	(6.2E−4)	3.11E−3	(1.1E−3)
1.0	0.0413	(4.5E−3)	0.0740	(1.7E−2)	0.0466	(5.9E−3)	0.0680	(1.5E−2)	6.12E−3	(1.2E−3)	6.30E−3	(2.1E−3)
1.5	0.0347	(1.0E−2)	0.0542	(1.2E−2)	0.0538	(8.4E−3)	0.0689	(1.5E−2)	6.29E−3	(1.1E−3)	7.84E−3	(1.8E−3)
2.0	0.0312	(1.0E−2)	0.0400	(9.0E−3)	0.0489	(7.9E−3)	0.0584	(1.3E−2)	5.36E−3	(1.0E−3)	9.58E−3	(2.2E−3)

this influences sputtering, we cannot exclude it. Another possible explanation is the difference of impurity content (e.g. O) between the bulk samples and the deposited layers. Our layers have a small oxygen content of a few at.% (see Section 2.1). It remains an interesting, but for the time being open question, whether the observed differences in the sputtering yield measured for of our sputter-deposited thin films and published data for bulk materials is a hint to a systematic deviation or just a consequence of experimental uncertainties. Another interesting aspect of this is the fact, that in plasma-surface-interaction processes in fusion devices a significant fraction of eroded surface material is re-deposited forming re-deposited layers. The here investigated sputter-deposited layers can be considered as a model system for such re-deposited layers. These issues will be addressed in future studies.

The experimental data (including both, the weight loss and RBS data) were fitted with the well-known empirical Bohdansky formula [12], which was developed based on the analytical sputtering theory by Sigmund [13]. Accordingly, the sputter yield Y is given as:

$$Y(E) = QS_n(\varepsilon)\left(1-\left(\frac{E_{th}}{E}\right)^{\frac{2}{3}}\right)\left(1-\frac{E_{th}}{E}\right)^2$$

where Q is the yield pre-factor, $S_n(\varepsilon)$ is the nuclear stopping cross section, E is the projectile energy and E_{th} is the threshold energy of the sputtering. For this fitting, $S_n(\varepsilon)$ was calculated with using the Kr-C interaction potential model [14], i.e.,

$$S_n(\varepsilon) = \frac{0.5\ln(1+1.2288\varepsilon)}{\varepsilon + 0.1728\sqrt{\varepsilon} + 0.008\varepsilon^{0.1504}}$$

with the reduced energy ε of

$$\varepsilon = E\frac{M_2}{M_1+M_2}\frac{a_L}{Z_1Z_2e^2}$$

as proposed by García-Rosales et al. [15]. M_1 and M_2 are the masses and Z_1 and Z_2 are the atomic numbers of the projectile and the target atoms, respectively. e is the electron charge and α_L is the Lindhard screening length given as

$$a_L = \left(\frac{9\pi^2}{128}\right)^{\frac{1}{3}} a_B\left(Z_1^{2/3}+Z_2^{2/3}\right)^{-\frac{1}{2}}$$

where α_B is the Bohr radius ($\alpha_B = 5.2917\times10^{-11}$ m). In many cases Q and E_{th} are used as free fitting parameters. However, in this work, E_{th} was not taken as a free parameter but determined by

$$E_{th} = \frac{E_{sb}}{\gamma(1-\gamma)},$$

with

$$\gamma = \frac{4M_1M_2}{(M_1+M_2)^2}.$$

E_{sb} is the surface binding energy of the target material. In general, it is taken equal to the heat of sublimation, which is a known

Table 2
Summary of surface binding energy E_{sb} and sputtering threshold energy for D ion bombardment E_{th} used in the fitting procedure as well as the obtained pre-factor Q for each target element.

	Surface binding energy: E_{sb} [eV]	Threshold energy: E_{th} [eV]	Fitting factor: Q
Cr	4.12	33.7	0.179
Fe	4.34	37.5	0.154
W	8.68	216	0.034

value, and here, the E_{sb} values are taken from Ref. [9]. In this work, accordingly, the pre-factor Q was the only free parameter to fit the experimental data. It is sometimes argued that the empirical Bohdansky formula is not always perfect to reproduce the experimental result over a large energy range. However, the fitting is very reasonable for all three elements investigated here (see Fig. 3). Values of E_{sb}, and E_{th} used in this study, and Q obtained by this fitting procedure are summarized in Table 2.

3.2. Comparison with other analytical formulae

Other analytical descriptions of sputtering yields which are widely accepted in the community today are semi-empirical formulae proposed by Eckstein et al. [16–18] and Yamamura et al. [19] (see Appendix). Eckstein's formula is based on the Bohdansky formula, but revised to improve the yield description, particularly, near the threshold energy. The Yamamura formula is based on Sigmund's sputtering theory as well as on the Bohdansky formula. The first Yamamura formula was better suited to reproduce sputtering for cases of heavy-ion projectiles [20]. It was later modified to extend it to the cases of light-ion projectiles where the particle reflection plays an important role for the sputtering [19,21]. In general, a drawback in using these formulae for evaluation of experimental data is that there are multiple free parameters for the fitting. It is not simple to determine the parameter combinations unambiguously. For this reason the empirical Bohdansky formula is applied for fitting the sputtering yield in this study. Nevertheless, both Eckstein and Yamamura have provided parameter combinations for a large number of projectile-target cases by fitting their formulae to theoretical results determined using their own simulation codes based on the binary collision approximation (BCA), i.e., TRIM.SP [22] and ACAT [23], respectively. In Fig. 3, yield curves from those analytical formulae with given fitting parameters (see Appendix) are shown as well. In general, both formulae show similar sputtering yields and reproduce the experimental data acceptably. Particularly, the Eckstein curve fits almost perfectly to this experimental data near the threshold energy.

3.3. Comparison with BCA-based calculation codes

As mentioned, benchmarking and validation of BCA-based calculation codes is one of the major objectives of this study. In this respect, the present experimental data are additionally compared with results from the calculation codes SDTrimSP [24] and SRIM [25].

The SDTrimSP code is based on the static Monte-Carlo simulation code TRIM.SP [22] and its dynamic version TRIDYN [26]. The latter allows dynamic simulations taking stoichiometry changes as a function of fluence into account. In this study, the sputtering calculation was performed with SDTrimSP version 5.00 [27]. The program provides a number of input parameters and allows selecting several options for performing the simulations. For calculation of the sputtering yield the decisive parameters are the surface binding energy and the interaction potential. The surface binding energy for each target material used in this study were the known heats of sublimation, i.e., the same values as listed in Table 2, and the Kr-C potential (default in SDTrimSP) was chosen as interaction potential. Other important calculation options were also set to default, e.g., the MAGIC method [28] was used for calculation of the scattering integral, and the inelastic stopping power was treated by equipartition of Lindhard-Scharff [29] and Oen-Robinson [30] models.

SRIM [25] is probably the most widely distributed calculation program used for various purposes, such as ion range, damage cascade profile and sputtering simulations. In this study, the sputtering was calculated using the "Calculation of Surface Sputtering" option in the SRIM-2013 package. Surface binding energy is also an input variable in SRIM, but the heat of sublimation is set as the default value. For the calculation presented here, the surface binding energies used in SRIM were identical to those used in the SDTrimSP calculations.

Fig. 4 shows the comparison between code calculation results and the present experimental data. The SDTrimSP outputs for Fe and Cr show yields close to the experimental results, agreeing within $\pm 20\,\%$ in most of the measured energy range. For W, the SDTrimSP results are somewhat higher than the experimental data. Nevertheless, the difference is still within $\sim 50\,\%$ in the measured energy range. Overall, one can conclude that SDTrimSP results are in reasonable agreement with the experimental results for all three investigated elements. On the other hand, SRIM simulation results disagree in some cases substantially from the experimental data. Although the results for Fe and Cr agree reasonably with the experimental results for energies above ~ 300 eV/D, in both cases the yields deviate significantly in the lower energy range close to the threshold energy. Namely, the drop of the sputtering yield occurs at much higher energies than in the experimental data and in the SDTrimSP results. The SRIM result for W also shows the similar deviation around the threshold energy. Furthermore, in the case of W, it shows a relatively large difference also in the energy range above 500 eV/D, i.e., the W sputtering yield calculated by SRIM is always higher than the experimental results by more than a factor of 2.

The strong deviation of the SRIM results found near the threshold energy can lead to a severe underestimation of the real sputtering yield in that energy range. As mentioned above, one could vary the surface binding energy for the SRIM sputtering calculation trying to improve the agreement, but the simulations with reduced surface binding energies did not lead to a notable improvement for all three investigated elements. Another possible explanation for the differences between SRIM and SDTrimSP could be the chosen interaction potential in the simulations. In SRIM, the interatomic interaction and inelastic stopping power are approximated using the Ziegler-Biersack-Littmark (ZBL) universal potential model [25]. Hofsäss et al. recently pointed out that it seems that the ZBL potential has some limitations to describe low energy binary collisions [31]. Since SDTrimSP allows choosing different interaction potentials, we tested the influence of the used potential model within SDTrimSP by comparing results for the ZBL potential with those for the Kr-C potential. Compared to the Kr-C potential, the simulation with the ZBL potential provides worse agreement with the experimental results. Sputtering yields calculated for Fe and W (Cr was not checked) using the ZBL potential were systematically

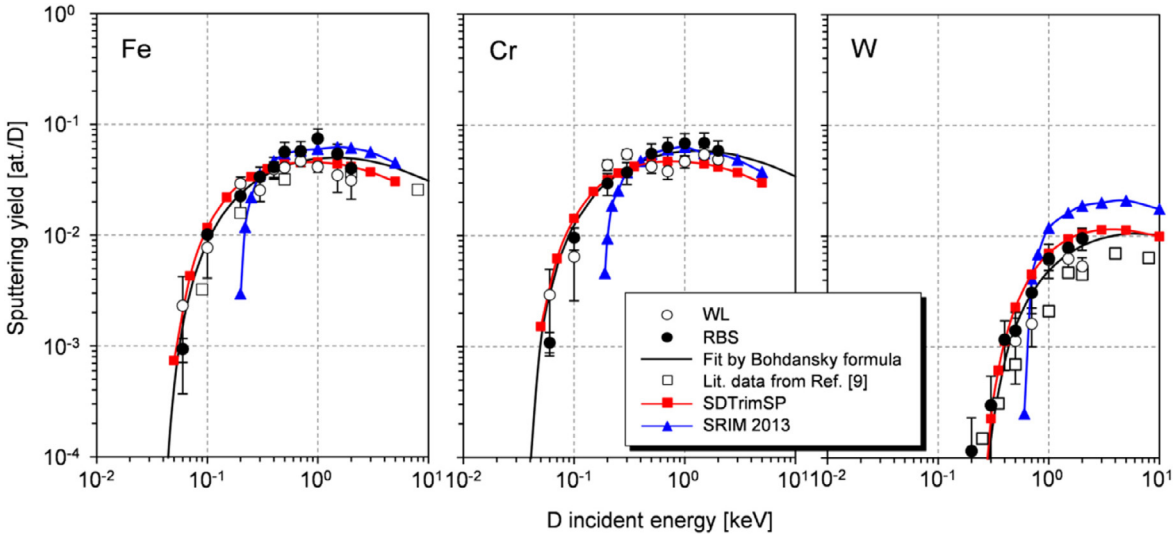

Fig. 4. Comparison between experimental data obtained in this study and literature data [9], and data calculated by BCA-based simulation codes: SDTrimSP and SRIM.

higher by about 40 % compared with the yields calculated with the Kr-C potential which are for W already up to 50 % higher than the current experimental data. Nevertheless, in SDTrimSP, the ZBL potential gives still finite yield values in the energy range around the threshold in contrast to SRIM which showed 0 yield in that energy range. This means that the used potential model can somewhat influence the sputtering simulation; however, it is not the reason explaining the observed difference between SRIM and SDTrimSP in the energy range at and slightly above the threshold. This comparison indicates that SRIM has some other intrinsic deficiencies for calculating sputtering yields near the threshold energy.

4. Summary

Sputtering yields of RAFM-related materials: Fe, Cr and W by energetic D ion bombardment were measured by means of the thin film technique under well-defined laboratory conditions. The bombardment energy range was from 60 to 2000 eV/D, which is relevant for the ion-material interaction in fusion devices. Comparison with published data for Fe and W shows that the here presented data agree with the published data within the experimental uncertainties; however, the yields for sputter-deposited films seem to be systematically higher than the published data which were measured for bulk materials. It remains to be investigated whether this is a real effect or an expression of the general experimental uncertainty.

The measured data were evaluated with a conventional semi-empirical fit formula suggested by Bohdansky et al. [12]. Experimental results are well fitted by the Bohdansky formula. Furthermore, it was confirmed that analytical formulae suggested by Eckstein et al. and Yamamura et al. with given fitting parameters (see Appendix) also agree acceptably with the experimental data.

Comparison with BCA-based calculation codes shows that SDTrimSP provides a reasonable description of the sputter yields as a function of ion energy whereas SRIM calculation results shows a significant underestimation near the threshold energy. This indicates that SRIM has some limitations to describe the low energy binary collision, and accordingly, SDTrimSP is better suited to simulate sputtering yields in the fusion-relevant energy range.

Acknowledgments

The authors acknowledge J. Dorner, M. Fußeder, F. Koch and A. Weghorn for their technical assistances. This work has been carried out within the framework of the EUROfusion Consortium and has received funding from the Euratom research and training programme 2014–2018 under grant agreement No 633053. The views and opinions expressed herein do not necessarily reflect those of the European Commission. Work performed under EUROfusion WP PFC.

Appendix

In Eckstein's formula [16–18], the sputtering yield *Y(E)* is given as

$$Y(E) = QS_n(\varepsilon)\frac{\left(\frac{E}{E_{th}}-1\right)^{\mu}}{\frac{\lambda}{\omega(\varepsilon)}+\left(\frac{E}{E_{th}}-1\right)^{\mu}}.$$

The pre-factor Q and the nuclear stopping cross-section $S_n(\varepsilon)$ are the same as in the Bohdansky formula, while the term dealing with the threshold is modified and two additional fitting parameters: λ and μ are introduced. $\omega(\varepsilon)$ is given as

$$\omega(\varepsilon) = \varepsilon + 0.1728\sqrt{\varepsilon} + 0.008\varepsilon^{0.1504}$$

with the reduced energy ε as defined in the body of the text.

The Yamamura [19] formula is given as

$$Y(E) = 0.042Q\frac{\alpha(M_2/M_1)}{E_{sb}}\frac{S_n(\varepsilon)}{1+\Gamma S_e\varepsilon^{0.3}}\left(1-\sqrt{\frac{E_{th}}{E}}\right)^{s}$$

where

$$\alpha\left(\frac{M_2}{M_1}\right) = 0.249\left(\frac{M_2}{M_1}\right)^{0.56} + 0.0035\left(\frac{M_2}{M_1}\right)^{1.5}$$

and the term Γ is

$$\Gamma = \frac{W}{1+\left(\frac{M_1}{7}\right)^3}.$$

The nuclear stopping cross section $S_n(\varepsilon)$ used in Yamamura formula is a modified Thomas-Fermi approximation given as

$$S_n(\varepsilon) = 8.478\frac{Z_1Z_2}{\sqrt{Z_1^{\frac{2}{3}}+Z_2^{\frac{2}{3}}}}\frac{M_1}{M_1+M_2} \times \frac{3.441\sqrt{\varepsilon}\ln(\varepsilon+2.718)}{1+6.355\sqrt{\varepsilon}+\varepsilon\left(6.882\sqrt{\varepsilon}-1.708\right)},$$

Table 3
Fitting parameters for Eckstein [18] and Yamamura [19] formulae. Parameters are all given by the respective author.

	Eckstein formula [18]				Yamamura formula [19]			
	Q	E_{th} [eV]	λ	μ	Q	E_{th} [eV]	W	s
Cr	0.1084	35.0	0.2899	1.7152	0.93	35.0	1.44	2.5
Fe	0.0919	40.9	0.2743	1.3489	0.75	38.6	1.2	2.5
W	0.0183	228.8	0.3583	1.441	0.72	222.0	2.14	2.8

with the reduced energy ε, as defined in the body of the text. S_e is the Lindhard inelastic stopping coefficient given as

$$S_e = \left(\frac{9\pi^2}{128}\right)^{\frac{1}{3}} \frac{(M_1+M_2)^{\frac{3}{2}}}{M_1{}^{\frac{3}{2}}\, M_2{}^{\frac{1}{2}}} \frac{Z_1{}^{\frac{3}{2}}\, Z_2{}^{\frac{1}{2}}}{\left(Z_1{}^{\frac{1}{3}} + Z_2{}^{\frac{2}{3}}\right)^{\frac{3}{4}}}.$$

Accordingly, Q, W and s are parameters for fitting.

As mentioned in the body of the text, both authors have given the fitting parameters for each projectile-target combination in Refs. [18,19], as listed in Table 3.

References

[1] J. Roth, E. Tsitrone, A. Loarte, et al., J. Nucl. Mater. 390–391 (2009) 1–9.
[2] C.H. Skinner, et al., Fus. Sci. Eng. Technol. 54 (2008) 891–945.
[3] B. van der Schaaf, F. Tavassoli, C. Fazio, et al., Fusion Eng. Des. 69 (2003) 197.
[4] V.M. Chernov, M.V. Leonteva-Smirnova, M.M. Potapenko, et al., Nucl. Fusion 47 (2007) 839–848.
[5] S. Jitsukawa, M. Tamura, B. van der Schaaf, et al., J. Nucl. Mater. 307–311 (2002) 179–186.
[6] Q. Huang, FDS Team, J. Nucl. Mater. 455 (2014) 649–654.
[7] D. Maisonnier, I. Cook, S. Pierre, et al., Fusion Eng. Des. 75–79 (2005) 1173.
[8] J. Roth, K. Sugiyama, V. Alimov, et al., J. Nucl. Mater. 454 (2015) 1.
[9] W. Eckstein, C. García-Rosales, J. Roth, W. Ottenberger, "Sputtering data", (1993), IPP Report 9/82, Max-Planck-Institut für Plasmaphysik, Garching, (http://hdl.handle.net/11858/00-001M-0000-0027-6324-6).
[10] R.C. Davis, T.C. Jemigan, O.B. Morgan, et al., Rev. Sci. Instrum. 46 (1975) 576.
[11] M. Mayer, "SIMNRA user's guide", (1997), IPP Report 9/113, Max-Planck-Institut für Plasmaphysik, Garching, (http://hdl.handle.net/11858/00-001M-0000-0027-6157-F).
[12] J. Bohdansky, Nucl. Instr. and Meth. B 2 (1984) 587.
[13] P. Sigmund, Phys. Rev. 184 (1969) 383.
[14] W.D. Wilson, L.G. Haggmark, J.P. Biersack, Phys. Rev. B 15 (1977) 2458.
[15] C. García-Rosales, W. Eckstein, J. Roth, J. Nucl. Mater. 218 (1994) 8–17.
[16] W. Eckstein, R.Preuss, J. Nucl. Mater. 320 (2003) 209.
[17] W. Eckstein, Vacuum 82 (2008) 930.
[18] R. Behrisch, W. Eckstein, Sputtering by particle bombardment, experiments and computer calculations from threshold to MeV energies, Topics in Applied Physics, 110, Springer, 2007.
[19] Y. Yamamura, H. Tawara, Atom Data Nucl. Data Tables 62 (1996) 149.
[20] Y. Yamamura, Radiat. Eff. 55 (1981) 49.
[21] Y. Yamamura, N. Matsunami, N. Itoh, Radiat. Eff. 71 (1983) 49.
[22] J.P. Biersack, W. Eckstein, Appl. Phys. A 34 (1984) 2.
[23] Y. Yamamura, Y. Mizuno, IPPJ-AM-40, Nagoya University (1985).
[24] W. Eckstein, R. Dohmen, A. Mutzke, R. Schneider, "SDTrimSP: A Monte-Carlo code for calculating collision phenomena in randomized targets", IPP Report 12/3 (2007), Max-Planck-Institut für Plasmaphysik, Garching, (http://hdl.handle.net/11858/00-001M-0000-0027-04E8-F).
[25] J.F. Ziegler, J.P. Biersack, M.D. Ziegler, "SRIM The stopping and ranges of ions in matter", SRIM Co. (2008), (http://www.srim.org/).
[26] W. Möller, W. Eckstein, J.P. Biersack, Comput. Phys. Commun. 51 (1988) 355.
[27] A. Mutzke, R. Schneider, W. Eckstein. and R. Dohmen, "SDTrimSP version 5.00", IPP Report 12/08 (2011), Max-Planck-Institut für Plasmaphysik, Garching, (http://hdl.handle.net/11858/00-001M-0000-0026-EAF9-A).
[28] J.P. Biersack, L.G. Haggmark, Nucl. Instr. and Meth. 174 (1980) 257.
[29] J. Lindhard, M. Scharff, Phys, Rev. 124 (1961) 128.
[30] O.S. Oen, M.T. Robinson, Nucl. Instr. and Meth. 132 (1976) 647.
[31] H. Hofsäss, K. Zhang, A. Mutzke, Appl. Surface Sci. 310 (2014) 134.